water

MDPI

Article

Identification of Potential Landslide Hazards Using Time-Series InSAR in Xiji County, Ningxia

Jia Zhang [1,2,*], Yongfeng Gong [1,2], Wei Huang [2], Xing Wang [3,4,5], Zhongyan Ke [6], Yanran Liu [3,4,5], Aidi Huo [3,4,5,*], Ahmed Adnan [3,4,5] and Mohamed EL-Sayed Abuarab [7]

1 School of Environmental Studies, China University of Geosciences, Wuhan 430074, China
2 NingXia Survey and Monitor Institute of Land and Resources, Yinchuan 750001, China
3 Key Laboratory of Subsurface Hydrology and Ecological Effects in Arid Region of the Ministry of Education, Chang'an University, Xi'an 710054, China
4 School of Water and Environment, Chang'an University, Xi'an 710054, China
5 Xi'an Monitoring, Modelling and Early Warning of Watershed Spatial Hydrology International Science and Technology Cooperation Base, Chang'an University, Xi'an 710054, China
6 School of Humanities, Chang'an University, Xi'an 710054, China
7 Faculty of Agriculture, Cairo University, Giza 12613, Egypt
* Correspondence: flyzjsel@163.com (J.Z.); huoaidi@chd.edu.cn (A.H.)

Abstract: Potential landslide identification and monitoring are essential to prevent geological disasters. However, in mountainous areas where the surface gradient changes significantly, the leveling effect is not completely removed, affecting the deformation results. In this paper, the SBAS-InSAR and PS-InSAR time-series processing methods were combined to interfere with the SAR image data of the ascending orbit in the southern mountainous area of Ningxia and its surrounding regions. Based on the obtained surface deformation monitoring results and optical images, landslide hazard identification was successfully carried out within the coverage area of 3130 km^2 in Xiji County. The results show that the whole study area presented a relatively stable state, most of the deformation rates were concentrated in the range of 0 mm/a to −10 mm/a, and the deformation in the southwest area was larger. A total of 11 large potential landslides (which were already registered potential danger points of geological disasters) were identified in the study area, including three historical collapses. The landslide identification results were highly consistent with the field survey results after verification. The timing analysis of the typical landslide point of the Jiaowan landslide was further carried out, which showed that the Jiaowan landslide produced new deformation during the monitoring time, but it was still in a basically stable state. It can do a good job in disaster prevention and reduction while strengthening monitoring. The results of this study have a guiding effect on landslide prevention and mitigation in the mountainous areas of southern Ningxia.

Keywords: southern mountainous region of Ningxia; time-series InSAR; potential landslide identification; spatiotemporal characteristics

Citation: Zhang, J.; Gong, Y.; Huang, W.; Wang, X.; Ke, Z.; Liu, Y.; Huo, A.; Adnan, A.; Abuarab, M.E.-S. Identification of Potential Landslide Hazards Using Time-Series InSAR in Xiji County, Ningxia. *Water* **2023**, *15*, 300. https://doi.org/10.3390/w15020300

Academic Editor: Achim A. Beylich

Received: 17 December 2022
Revised: 3 January 2023
Accepted: 5 January 2023
Published: 11 January 2023

1. Introduction

The early identification of any hazard's risk is one of the essential technical means to prevent and control geological disasters [1]. For steep mountainous regions and areas with high vegetation coverage which are difficult to reach by manual investigation, early landslide risk identification can solve the problem that the number of potential danger points is not clear, which has a good role in early disaster warning and risk management [2]. In recent years, Interferometric Synthetic Aperture Radar (InSAR) technology has been continuously mainstream, with the advantages of being all-weather, having an extensive range, and having a high accuracy, which play a vital role in promoting the development of landslide hazard risk assessment [3–5]. The traditional time-series InSAR techniques are used to identify the landslide with Differential Interferometric Synthetic Aperture

Radar (D-InSAR), Small Baseline Subset Interferometric Synthetic Aperture Radar (SBAS-InSAR), and Permanent Scatterer Interferometric Synthetic Aperture Radar (PS-InSAR). D-InSAR technology processes two or three scene image data, which can quickly obtain the deformation results but cannot obtain long time-series of surface deformation information. SBAS-InSAR technology is suitable for distributed target analysis and can obtain large-area deformation information. PS-InSAR is suitable for point-target analysis and can extract PS points with high reliability [6,7]. InSAR technology can be used for the efficient early identification of regional geological disasters [8].

The application of comprehensive remote sensing measurement technologies such as InSAR and optical remote sensing significantly impacts the early identification of potential landslides in large areas and the assessment of slope risks [9–12]. Zhao et al. [13] delineated some potential landslide hazards in the Bailong River basin through InSAR technology and verified the reliability of InSAR technology. Wang et al. [14] identified 144 potential landslide points in Datong County, Qinghai Province, based on InSAR and optical remote sensing technology, indicating the feasibility of InSAR technology for large-scale landslide monitoring. Li [15] used InSAR technology to monitor the landslide in the middle reaches of the Bailong River and analyzed the landslide distribution and deformation law in this area. Zhao et al. [16] used SAR data to monitor the deformation of the Heifangtai landslide in Gansu and studied the landslide instability mode. Xu [17] proposed building a "three investigations" system and achieved good results in landslide monitoring by using optical remote sensing, InSAR, UAV aerial photography, and other technologies. Zhang et al. [18] successfully warned of the sudden loess landslide in Yongjing County, Gansu Province, 6 h in advance by combining InSAR technology and the GNSS monitoring system. This successful warning has laid the foundation for subsequent landslide monitoring. Although InSAR technology is increasingly used in landslide identification and tracking, it is still challenging to identify landslides in mountainous areas with large terrains and high vegetation coverage due to the influence of spatiotemporal incoherence [19]. Therefore, InSAR technology's identification effect and applicability for potential landslides in mountainous areas need further in-depth analysis. The innovation of this study is to combine the advantages of SBAS-InSAR technology and PS-InSAR technology in extracting deformation information. The early identification of potential landslides in the southern mountainous areas of Ningxia effectively overcomes the limitations of time and space caused by topography. The flat effect is better eliminated, and the surface deformation results with higher accuracy are obtained, which shows the feasibility of InSAR technology in the high-precision identification and monitoring of potential landslides in the southern mountainous areas of Ningxia.

The mountainous areas of southern Ningxia are part of the Northwest Loess Plateau. The mountains and plains in this area are scattered, the height difference fluctuates wildly, and the surface gullies are crisscrossed. Therefore, it is a highly susceptible area to geological disasters in Ningxia. Xiji County is located in the mountainous region of southern Ningxia. The landform is mainly loess hills, followed by laterite hills. The geological environment is complex and prone to geological disasters [20–22]. The landslide risk is 79% of the total geological disasters in Xiji County. In this paper, Xiji County was taken as the study area, and PS and SBAS fusion technologies were used to conduct interference processing on the Sentinel-1A ascending orbit data in the region from 2018 to 2021. High-precision surface deformation results in the region were obtained. The potential landslide area was delineated in the deformation results by the visual interpretation of optical images, and a field inspection was carried out to check the reliability and effectiveness of the identification results. The field survey of the typical Jiaowan landslide group has provided adequate data support and method reference for the prevention and control of geological disasters, such as the early identification, monitoring and early warning, management, relocation, and avoidance of geological hazards in the southern mountain areas of Ningxia.

2. Study Area

Xiji County is located in the southern mountainous area of the Ningxia Hui Autonomous Region (105°20′-106°04′, 35°35′-36°14′). The county has convenient transportation, with an east–west length of about 67 km, a north–south width of about 74 km, and a total area of 3130 km^2 (Figure 1). Three seasonal rivers are developed in the county, including the Qingshui River, Hulu River, and Zuli River. According to the local geomorphic characteristics, it can be divided into three secondary geomorphic units: the loess hilly and gully area, earth rock mountain area, and river valley. The hilly loess area accounts for 83% of the total area. The terrain is high in the north, low in the south, high in the east, and low in the west. The altitude is between 1656 and 2606 m. Xiji County has a fragile ecological environment, with an average annual temperature of 12.7 °C and an average annual precipitation of 570.2 mm. Precipitation is mainly concentrated from July to September. The land types in the county are complex and diverse, with deep soil layers and loose soil quality. Affected by the 1920 Haiyuan earthquake, which had a magnitude of 8.5, a large number of new landslides were formed in Xiji County after the earthquake. At the same time, due to the impact and damage of the earthquake, the rock and soil mass structure in some parts of the area is loose, which increases the possibility of collapses and landslides in the area [23].

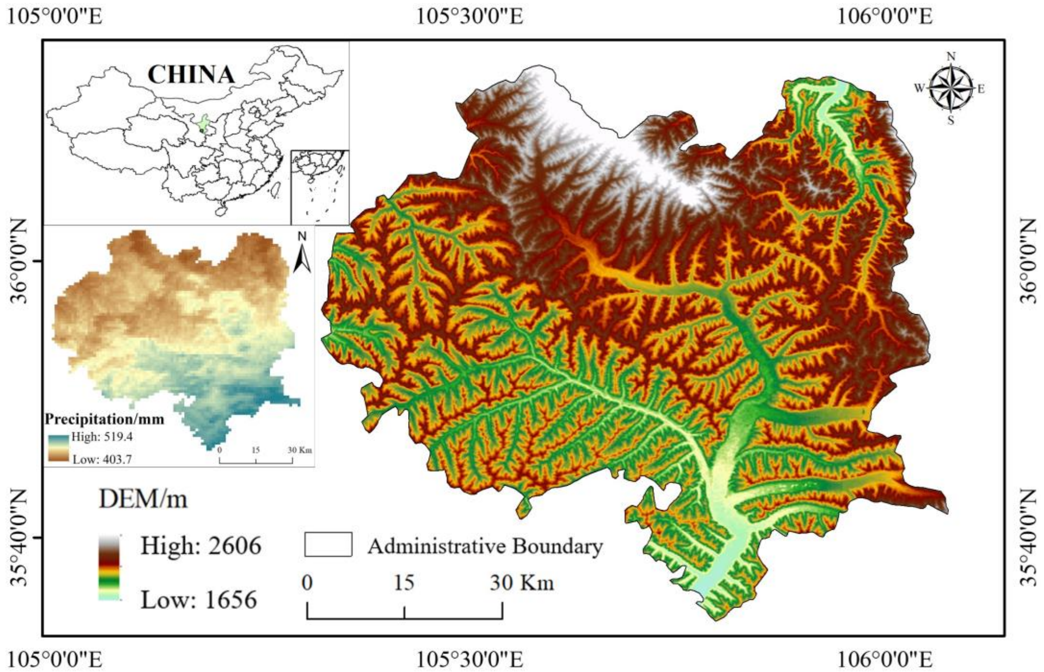

Figure 1. Location map of Xiji County.

3. Data and Methods

3.1. Experimental Data

The data required for this experiment are: Sentinel-1A satellite image data, Digital Elevation Model (DEM) data, Sentinel satellite precision orbit files, and optical remote-sensing image data. The Sentinel-1 satellite is two earth-monitoring satellites launched by Global Monitoring for Environment and Security (GMES) in 2014 and 2016, respectively. The two satellites take a 12-day cycle to image the earth's all-weather day and night radar, with a width of 250 km, and are mainly used in landslides, urban land subsidence, and other aspects. The Sentinel satellite image data download website is as follows: https://search.asf.alaska.edu/ (accessed on 15 August 2021). The data center provides dual satellite images in the same orbit for free. DEM (SRTM) data can give reference terrain with a spatial resolution of 90 m. Its download website is https://srtm.csi.cgiar.org/ (accessed on 15 August 2021). Sentinel satellite precision orbital file data can correct orbital error information. The download website is http://www.gscloud.cn/ (accessed on 15 August 2021). The optical remote-sensing image data is the sky map image. The image was taken on 27 March 2021, with a resolution of 0.48 m. A total of 28 Sentinel-1A data scenes were selected from December 2018 to June 2021. The data type is Single Look Complex (SLC), the data mode is Interferometric Wide (IW), the track direction is ascending orbit, the spatial resolution is 5 × 20 m, and the incidence angle is 39.07°. The specific imaging time of images is shown in Table 1.

Table 1. Sentinel-1A image acquisition time.

Number	Image Date	Number	Image Date	Number	Image Date	Number	Image Date
1	18 December 2018	8	22 July 2019	15	30 March 2020	22	24 December 2020
2	23 January 2019	9	20 September 2019	16	23 April 2020	23	24 January 2021
3	28 February 2019	10	26 October 2019	17	29 May 2020	24	22 February 2021
4	24 March 2019	11	19 November 2019	18	22 June 2020	25	25 March 2021
5	29 April 2019	12	25 December 2019	19	14 August 2020	26	23 April 2021
6	23 May 2019	13	30 January 2020	20	25 October 2020	27	24 May 2021
7	28 June 2019	14	23 February 2020	21	30 November 2020	28	17 June 2021

3.2. Time-Series InSAR Methods

The temporal InSAR technology can effectively overcome the time and space decoherence problem caused by traditional measurement methods, and can obtain a large range of high-precision and high-quality deformation information in the study area. The persistent Scatterers-InSAR (PS-InSAR) technique was proposed by Ferretti et al. [24] to carry out differential interferometry for point targets with high coherence. The basic principle is to select time-continuous multi-scene image data in the same area and select one scene from the image as the main image and the rest as the secondary images by setting an appropriate baseline threshold. After all images are registered with the main image, a time-series interference is generated, and stable, permanent scatterer points with high coherence are obtained from the study area. The differential interference phase of each permanent scatterer point is obtained with differential interference processing of the interference pair using DEM, which contains four components of the phase:

$$\varphi\_dint = \varphi\_dem + \varphi\_def + \varphi\_atm + \varphi\_noise \tag{1}$$

where φ_dint is the differential interference phase at each permanent scatterer point, φ_dem is the topographic phase due to DEM error, φ_def is the phase caused by surface deformation in the radar line of sight direction (LOS), φ_atm is the phase caused by atmospheric delay, and φ_noise is the noise phase. By analyzing the time-series of the permanent scatterers, the atmospheric, noise, DEM, and other phases in the differential interference phase are separated according to the characteristics of each phase component, and the surface deformation phase of each permanent scatterer point is obtained to accurately monitor the regional surface displacement change value. Through this method, the points with stable backscatter characteristics in the SAR image can be identified, and the errors caused by unstable GCP points (Ground Control Points) in the artificial selection process can be avoided.

Small Baseline Subset-Interferometric Synthetic Aperture Radar (SBAS-InSAR) is an InSAR time-series analysis method for distributed targets proposed by Berardino et al. [6] in 2002 and applied to research in the field of surface deformation time-series monitoring. The principle is to set a reasonable threshold based on the spatiotemporal baseline obtained from the same region's $N + 1$ scene SAR image data in a time sequence. Select a standard main image, and use the main image as a reference for other images to form countless small baseline sets and generate the differential interferogram. The least squares method and the singular value decomposition method of the matrix are used to solve the deformation time-series and deformation rate.

Assuming that $N + 1$ SAR images with image time arrangement $(t_0, \ldots, t_n)$ are obtained from the study area, and M differential interferometers can be obtained after processing, and M satisfies:

$$\frac{(N+1)}{2} \leq M \leq \frac{N(N+1)}{2} \tag{2}$$

Assuming that the two images are obtained at different times and t_a and t_b are interfered to obtain a differential interferogram j ($t_b > t_a$), then the phase value of interferogram j corresponding to a pixel point (azimuth x, distance r) can be expressed as:

$$\delta\phi_j(x,r) = \phi(t_b, x, r) - \phi(t_a, x, r) = \frac{4\pi}{\lambda}[d(t_b, x, r) - d(t_a, x, r)] \tag{3}$$

where ϕ is the interference phase, $j \in (1, 2, \ldots, M)$, λ is the radar wavelength, $d(t_b, x, r)$ and $d(t_a, x, r)$ are the deformation variables accumulated along the radar line of sight direction in time t_a and t_b with the initial time t_0 as the control ($d(t_0, x, r) = 0$).

In order to obtain a settlement sequence that conforms to the law and is more intuitive, the phase value of the j-th interferogram can be calculated by integrating the relevant time period for generating the interferogram with the average phase velocity. Then the average phase velocity and phase are respectively expressed as:

$$v_j = \frac{\phi_j - \phi_{j-1}}{t_j - t_{j-1}} \tag{4}$$

$$\sum_{k=t_a,j+1}^{t_b,j} t_k - t_{k-1} v_k = \delta\phi_j \tag{5}$$

where v is the average phase velocity; ϕ is the interference phase; t is the phase acquisition time; and $\delta\phi_j$ is the interference phase of the j-th differential interferogram.

Integrating the settlement velocity of each time period can obtain the surface sedimentation volume of each time period, which is manifested in the form of matrix integration:

$$Bv = \delta\phi \tag{6}$$

where, when the coefficient matrix B ($M \times N$) is full rank or deficient rank, the surface deformation rate of the study area can be solved by the least squares method and the singular value decomposition method, respectively. Then, the corresponding cumulative deformation variable can be obtained according to the surface deformation rate.

3.3. Monitoring of Surface Deformation in Mountainous Areas

The complex terrain, vertical and horizontal ravines, large fluctuation of elevation difference, and luxuriant vegetation in mountainous areas lead to the inability of traditional survey and monitoring methods to obtain regional surface damage, which affects the identification of geological hazards and risks. Although the PS technique is limited to linear deformation, GCP points with high coherence can be obtained; SBAS has a good application effect in analyzing distributed targets. Therefore, based on the complementary advantages of the two methods, this paper combines PS-InSAR and SBAS-InSAR technologies to obtain the surface deformation monitoring results. Compared with using the PS-InSAR or SBAS-InSAR technologies, it can effectively reduce the error caused by SAR data processing and increase the accuracy of the results. In data processing based on SBAS-InSAR technology, highly coherent GCP points obtained by PS-InSAR technology are introduced during orbital refining to remove residual phase information, better eliminate the flat-ground effect, and improve the accuracy of SBAS-InSAR technology processing results. The specific operation steps are as follows: (1) data preprocessing: due to the large amount of original data, the research area is cut to reduce data processing time and improve efficiency; (2) PS InSAR technology extracts highly coherent GCP points: set parameters such as deformation sampling frequency, residual height sampling frequency, spatiotemporal correlation filtering, and coherence coefficient threshold to reduce atmospheric phase error and obtain high-quality and stable GCP points; (3) SBAS-InSAR technology differential interference calculation: By setting a specific spatiotemporal baseline threshold value, the interference relative is generated. Then, registration, leveling, filtering, phase unwrapping and coherence calculations are performed to obtain the phase diagram and unwrapping diagram after de-leveling and filtering; (4) track refining and re-leveling: GCP points obtained by PS-InSAR technology are introduced to eliminate the leveling effect; (5) temporal domain deformation calculation: the atmospheric phase is effectively removed by two SBAS inversions to obtain the deformation rate and deformation quantity. The processing is shown in Figure 2.

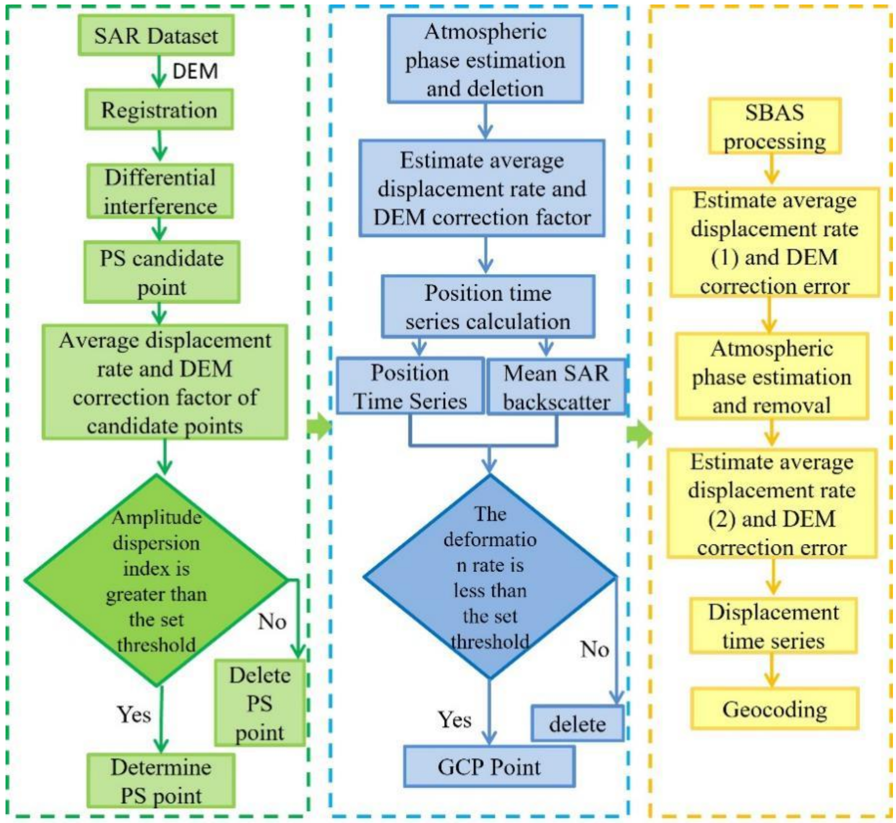

Figure 2. SBAS-InSAR technology framework integrating PS technology.

4. Result Analysis

4.1. Identification of Potential Landslide Hazards

SARScape5.2 software was used to process the data, the results were imported into the Arcgis10.3 software for density segmentation, and the optical remote-sensing image base map was added. Finally, the spatial variation map of the annual average deformation rate of the radar line of sight in Xiji County was obtained. According to the monitoring results of time-series InSAR technology, the number of coherence point targets (CTs) is 824,557, and the average coherence point density is about 262 CTs/km^2, which meets the requirements of landslide-related research [10]. Based on the slope's lithological characteristics, data inversion accuracy, field survey results, and previous study [12], ±10 mm/a was set as the threshold value of the landslide deformation rate of the radar line of sight (LOS). The potential landslide was identified with optical images, and the results shown in Figure 3 were obtained.

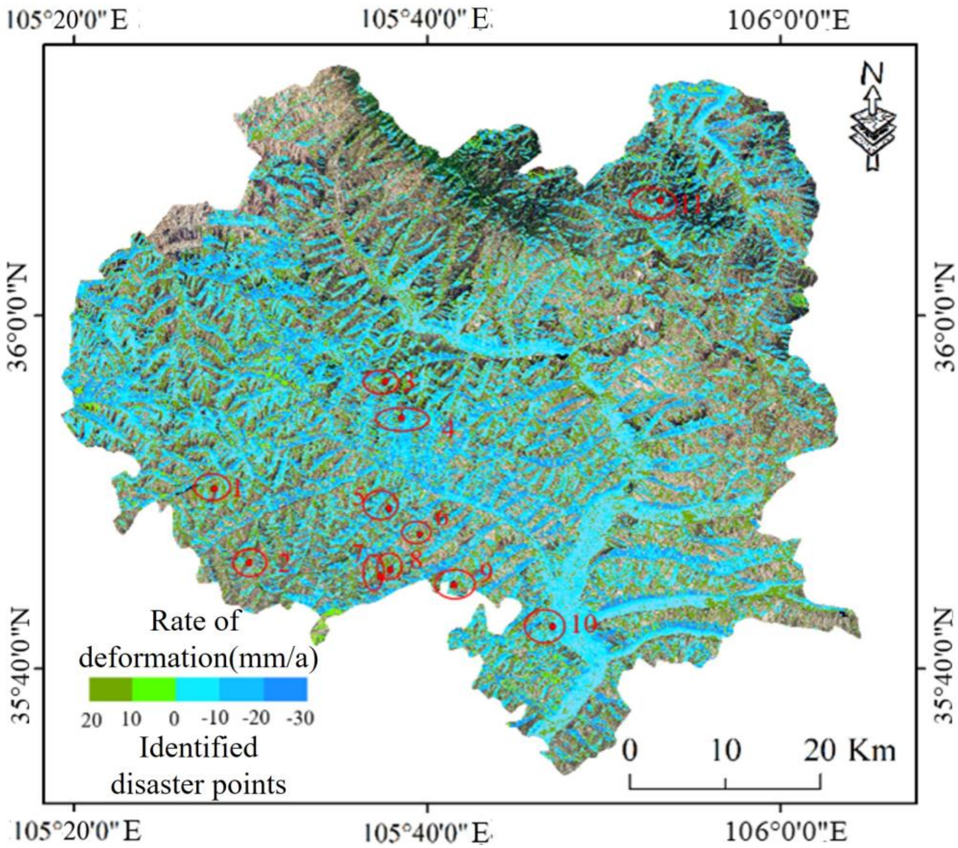

Figure 3. The annual average deformation rate on LOS.

In Figure 3, positive values indicate that the surface movement is close to the satellite direction, while negative values indicate that the surface movement is far away from the satellite direction. During the monitoring period from December 2018 to June 2021, the whole study area showed a relatively stable state, and most of the deformation rates were concentrated in the range of 0 mm/a to −10 mm/a. The slope on the southwest side was the main deformation area in Xiji County, and the maximum cumulative shape variable was −55 mm. A total of 11 potential landslide hazard points (which are already registered potential danger points) have been identified in the study area, including three historical collapses, all of which belong to slopes that have been damaged and deformed under natural and artificial conditions and are collectively referred to as unstable slopes in engineering geology [25,26]. The specific information of landslide hazard points is shown in Table 2. The frequency of atmospheric precipitation and crustal activity can induce slope geological disasters such as landslides and mudslides to a certain extent [27–29]. According to the survey, the frequency of heavy rainfall during 1996–1998 was high, and there were many landslides and collapses, which fully conforms to the characteristics of high frequency and intensity of precipitation in this period. The stratum in the county is dominated by Quaternary loess. Due to the highly developed vertical joints of the loess, the slope edges often form a tensile fracture zone parallel to the slope trend, which is several meters wide. In addition, the loess has a loose structure, high porosity, and unique loess collapsibility. During heavy rainfall, the infiltration rate of surface water is very fast. When the water content of the soil is significant, its tensile and shear strength is significantly reduced. Continuous precipitation leads to the constant infiltration of surface water on the slope, and eventually causes the occurrence of landslide disasters.

Table 2. Statistical information table for identifying landslide points.

Number	Length/m	Width/m	Thickness/m	Volume/m^3	Threat Object	Landslide Scale
1	100	600	5–10	3,825,000	Residential highway	Large loess landslide
2	200	300	5–10	3,062,500	Settlement	Large loess landslide
3	300	400	5–10	40,000	Settlement	Small loess landslide
4	210	470	25	2,438,800	Settlement	Large loess landslide
5	100	200	5–10	5,400,000	Settlement	Large loess landslide
6	200	200	5–15	5,390,000	Settlement	Large loess landslide
7	200	1000	10–15	13,062,500	Settlement	Giant loess landslide
8	1500	1000	25	37,500,000	Settlement	Giant loess landslide
9	500	950	25	11,875,000	Settlement	Giant loess landslide
10	300	1100	20	6,600,000	Residential highway	Large loess landslide
11	500	500	20	1,000,000	Settlement	Large loess landslide

4.2. Analysis of Spatiotemporal Characteristics of Typical Potential Landslides

The Jiaowan landslide is a large landslide group located in the Jiaowan Formation, Jiaowan Village, Pingfeng Town, Xiji County. Several major earthquakes mainly induced the landslide on the loess slope on the left bank of the Lanni River in 1920, 1970, and 2008. The slope is steep and covered with loess, the soil is broken, sinkholes have developed, and a small amount of Neogene red mudstone is exposed at the bottom of the gully facing the landslide front. According to the traditional landslide classification by Hungr et al. [30], the Jiaowan landslide belongs to soil creep. This area is a typical loess hilly and gully area. The loess beam moves to the northwest, and the terrain inclines from Southeast to Northwest. As a result, the hills and beams are undulating, the gully is crisscrossed, and landslides develop on the slopes of the loess hills. According to the InSAR results, the large landslide group produced new deformation within the monitoring time. The Jiaowan landslide was identified by combining optical remote-sensing interpretation and InSAR technology. The deformed areas in the Jiaowan landslide group were selected for analysis, as shown in Figure 4. The red boundary in Figure 4 represents the landslide range, Figure 4a is the optical image, and Figure 4b is the InSAR recognition result. The quantitative results obtained by InSAR are graded and displayed in different colors. The blue part of Figure 4b represents the settlement area. The deformation rate at Point 6# is 16 mm/a, and the deformation rate at Point 7# is 13 mm/a. Point 7# is located outside the boundary of the landslide, which is more likely to collapse.

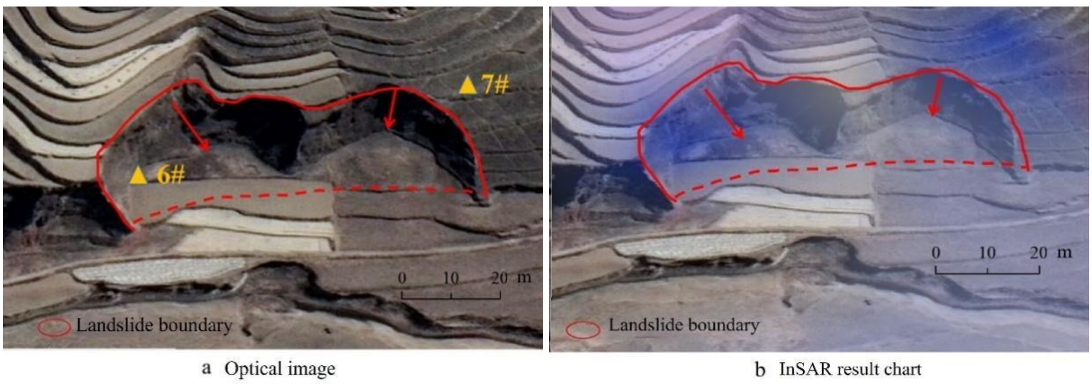

Figure 4. Jiaowan landslide. (**a**) optical image; (**b**) InSAR result chart.

In order to have a more intuitive and in-depth understanding of the deformation and causes of the Jiaowan landslide, an on-site investigation of the landslide was carried out. The red mark in Figure 5 shows the scope and movement direction of the landslide. The landslide is located to the northwest of Jiaowan Village, with a geographic location of 105°33′34″ E and 35°47′53″ N, as shown in Figure 5a. The landslide perimeter is clear and circular-shaped. The rear wall is steep, with an elevation of 2060 m and a height of about 25 m. The slope is steeper, with a slope of nearly 65°. When the slope is eroded by flowing water, new erosion ditches appear (Figure 5b), and the stability of the slope decreases. There are sinkholes on the slope wall (Figure 5c). The pavement around the landslide seriously collapsed (Figure 5d). The slippery soil is mainly silt, and the color is yellow-brown to black-brown. It has a homogeneous structure, the soil layer is loose, the shear strength is low, the vertical joints are cultivated, it contains silty sand and dark minerals, develops wormholes, and root pores have a low moisture content and are in a plastic state. The main lithology of the landslide bed is late Pleistocene loess, dark brown, with high moisture content and vertical joints. The earthquake mainly triggers the landslide. The river scours the front edge of the landslide, and creep occurs in the rainy season. The stratum in the landslide area is mainly composed of Pleistocene eolian loess and Quaternary landslide deposits. The rock and soil cracks develop, the physical and mechanical properties are poor, the soil is relatively broken, and the precipitation is easy to infiltrate, which may cause the overall instability of the landslide [31]. The prevention and control of the Jiaowan slope should focus on monitoring. If conditions permit, the front edge of the slope should be supplemented by protective works to reduce the erosion of the river. If signs of deformation are found, disaster prevention measures should be taken immediately.

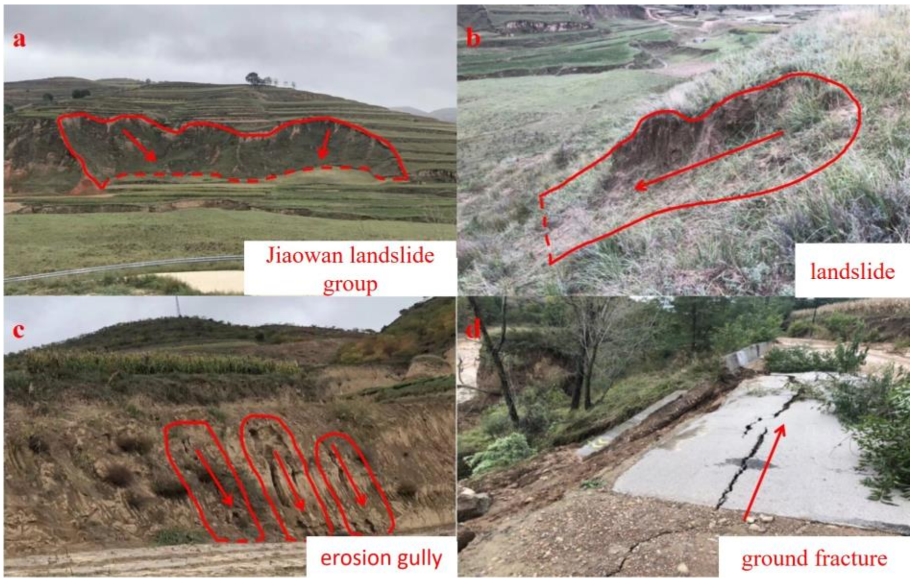

Figure 5. Field investigation. (**a**) Jiaowan landslide group; (**b**) landslide; (**c**) erosion gully; (**d**) ground fracture.

5. Discussion

The development and distribution of geological hazards in Ningxia have prominent regional characteristics closely related to landform and stratigraphic lithology. Landslides and collapses are mainly distributed in the hilly loess areas of southern Ningxia, mainly including soil landslides and loess gully bank collapses. Predecessors have completed much work monitoring geological disasters in south Ningxia using various technical means [32,33]. In summary, it is found that most of the loess hilly areas in Ningxia are loess landslides, especially the areas with underlying Tertiary argillaceous rocks; overlying thin layers of loess and seriously cut terrain are the most developed.

The landslide is mainly caused by natural and human factors, mainly including the influence of stratum and lithology, human engineering activities, and precipitation. The landslide events are easily triggered by intense rainstorms [34]. Compared with other areas, there is more precipitation in mountainous regions. The infiltration of rainwater into underground cracks further expands the cracks, and the osmotic pressure increases the possibility of landslides. As far as Xiji County is concerned, the fragmentation of the loess, the development of joints and fissures, and the very loose structure of the soil make it easy for surface water to seep down and eventually gather on the surface of the mudstone to form an obvious water barrier, forming the characteristics of a saturated cement belt developed along the sliding surface. Under the influence of frequent regional neotectonic activities and intensified human activities, the loess-red layer structure in this area has induced some new landslides [35]. Human factors, such as slope excavation, excessive reclamation, slope grazing, and other behaviors, directly change the surface environment, affect vegetation cover and precipitation infiltration, and increase the possibilities of collapses and landslides.

For landslide prevention and control, the cracks and sinkholes on the slope can be timely treated to prevent rainwater infiltration. The exposed slope easily infiltrates surface water, and the vegetation conditions on the slope should be improved by planting trees reasonably. There is a free face at the front of the slope, so all kinds of human engineering activities which may disturb the landslide should be avoided as far as possible, and excavation of the slope toe is strictly prohibited. The landslide land should be used reasonably. It is not suitable to build various water conservancy projects conducive to precipitation infiltration on the landslide and intercepting ditches, and other means can be set up around areas prone to landslides. Establish a landslide disaster monitoring network, strengthen the dynamic monitoring of old landslides in rainy seasons, and immediately report to the competent department when signs of deformation are found to formulate disaster prevention and emergency response measures.

6. Conclusions

Based on Sentinel-1A data, this paper carried out comprehensive monitoring and in-depth analysis of the landslide of Xiji County in the southern mountainous region of Ningxia. In addition, we conducted a time-series analysis on selected monitoring points of landslide hazards and studied the application method of time-series InSAR technology in the process of landslide identification monitoring. The conclusions are as follows:

(1) According to the fusion technology of PS and SBAS, the cumulative deformation volume and deformation rate of the surface from 2018 to 2021 were monitored. The results showed that the whole study area presented a relatively stable state, that the maximum cumulative deformation within the region was −55 mm, and that the southwest slope is the main deformation area in Xiji County.

(2) Early identification of potential landslides was carried out based on radar line-of-sight deformation rate maps and optical images, and 11 potential landslides (including three historical collapses) were identified in Xiji County, which is highly consistent with the field survey results. The feasibility and reliability of potential landslide identification for slope stability analysis are verified, which can provide certain data support for potential landslide investigation, the layout of major engineering facilities, and disaster prevention and reduction work in the region.

(3) The 11 potential landslide hazard points identified in this study all belong to the slope that has been damaged and deformed under natural and artificial conditions. Among them, the Jiaowan landslide is in a basically stable state at present, but creep phenomenon often occurs in the rainy season, especially the heavy rain season, and water accumulation is easy behind the slope.

Author Contributions: Conceptualization, W.H. and Y.L.; Methodology, Y.G. and A.H.; Software, Y.G. and Z.K.; Validation, X.W. and A.A.; Formal analysis, X.W.; Investigation, Z.K. and M.E.-S.A.; Resources, J.Z., Y.L. and M.E.-S.A.; Data curation, A.A.; Writing—original draft, J.Z. and W.H.; Writing—review and editing, A.H. All authors have read and agreed to the published version of the manuscript.

Funding: This work was supported by the Natural Science Foundation of Ningxia, China (Grants No. 2021AAC03429, 2021AAC03426, 2021AAC03425), the sixth Lift Engineering of young scientific and technological talents of Ningxia, and the National Natural Science Foundation of China (Grants No. 42261144749, 41877232 and 41790444).

Data Availability Statement: Not applicable.

Acknowledgments: The authors thank the four anonymous reviewers and the editor for their constructive comments, which significantly improved the quality of this article.

Conflicts of Interest: The authors declare no conflict of interest. The funders had no role in the design of the study; in the collection, analyses, or interpretation of data; in the writing of the manuscript; or in the decision to publish the results.

References

1. Ge, D.Q.; Dai, K.R.; Guo, Z.C.; Li, Z.H. Early Identification of Serious Geological Hazards with Integrated Remote Sensing Technologies: Thoughts and Recommendations. *Geomat. Inf. Sci. Wuhan Univ.* **2019**, *44*, 949–956. [CrossRef]
2. Zhang, W.; LI, Y.Y.; Zhang, T.L.; Gui, L.; Zhou, C. Remote Sensing Interpretation of Landslide Geological Hazards in High Vegetation Coverage Area Based on Hazard Sensitivity Analysis. *Saf. Environ. Eng.* **2019**, *26*, 28–35. [CrossRef]
3. Burgmann, R.; Rosen, P.; Fielding, E. Synthetic Aperture Radar Interferometry to Measure Earth's Surface Topography and Its Deformation. *Annu. Rev. Earth Planet. Sci.* **2000**, *28*, 169–209. [CrossRef]
4. Shi, F.C.; Tang, Z.H.; Chen, Y.B.; Zhu, F.; Ye, S. Spatial-temporal Evolution Characteristics and Causes of Land Subsidence in Typical Area of Eastern Guangdong Province. *Saf. Environ. Eng.* **2019**, *26*, 8–16. [CrossRef]
5. Rott, H.; Nagler, T. The contribution of radar interferometry to the assessment of landslide hazards. In *Natural Hazards and Oceanographic Processes from Satellite Data*; Singh, R.P., Shea, M.A., Eds.; Elsevier: Amsterdam, The Netherlands, 2006; pp. 710–719.
6. Berardino, P.; Fornaro, G.; Lanari, R.; Sansosti, E. A new algorithm for surface deformation monitoring based on small baseline differential SAR interferograms. *IEEE Trans. Geosci. Remote Sens.* **2002**, *40*, 2375–2383. [CrossRef]
7. Lanari, R.; Mora, O.; Manunta, M.; Mallorqui, J.J.; Berardino, P.; Sansosti, E. A small-baseline approach for investigating deformations on full-resolution differential SAR interferograms. *IEEE Trans. Geosci. Remote Sens.* **2004**, *42*, 1377–1386. [CrossRef]
8. Xu, S.; Wang, S.X.; Niu, R.Q. Identification of the Potential Landslide in Wushan–Fengjie in the Three Gorges Reservoir Area Based on InSAR Technology. *Saf. Environ. Eng.* **2020**, *27*, 32–38. [CrossRef]
9. Zhu, J.J.; Li, Z.W.; Hu, J. Research Progress and Methods of InSAR for Deformation Monitoring. *Acta Geod. Cartogr. Sin.* **2017**, *46*, 1717–1733.
10. Li, M.S.; Wang, T. *Time Series Insar Technology and Application*; Science Press: Beijing, China, 2014.
11. Li, X.E.; Zhou, L.; Su, F.Z.; Wu, W.Z. Application of InSAR technology in landslide hazard: Progress and prospects. *Natl. Remote Sens. Bull.* **2021**, *25*, 614–629.
12. Shi, X.G. *Method and Application of Landslide Surface Deformation Monitoring Based on On-Board Radar Remote Sensing*; Wuhan University: Wuhan, China, 2016.
13. Zhao, B.Q. *Surface Deformation Characteristics and Early Identification of Potential Landslides Based on InSAR Technology in Bailong River Basin*; Lanzhou University: Lanzhou, China, 2019.
14. Wang, Z.W. *Research on Landslide Identification Method of Datong County in Qinghai Based on SBAS-InSAR Technology*; Chengdu University of Technology: Chengdu, China, 2019.
15. Li, G.Y. *Landslide Identification and Monitoring in the Middle Reaches of Bailong River Using Sentinel-1A*; Nanjing Normal University: Nanjing, China, 2018.
16. Zhao, C.Y.; Liu, X.J.; Zhang, Q.; Peng, J.B.; Xu, Q. Research on Loess Landslide Identification, Monitoring and Failure Mode with InSAR Technique in Heifangtai, Gansu. *Geomat. Inf. Sci. Wuhan Univ.* **2019**, *44*, 996–1007. [CrossRef]
17. Xu, Q. Understanding and Consideration of Related Issues in Early Identification of Potencial Geohazards. *Geomat. Inf. Sci. Wuhan Univ.* **2020**, *45*, 1651–1659. [CrossRef]
18. Chi, Y. Early warning, Beidou/GNSS monitoring system to avoid casualties. *Space Explor.* **2019**, *39*, 5.
19. Zhang, Y.; Meng, X.M.; Chen, G.; Qiao, L.; Zeng, R.Q.; Chang, J. Detection of geohazards in the Bailong River Basin using synthetic aperture radar interferometry. *Landslides* **2016**, *13*, 1273–1284. [CrossRef]
20. Huo, A.; Zhao, Z.; Luo, P.; Zheng, C.; Peng, J.; Abuarab, M.E.-S. Assessment of Spatial Heterogeneity of Soil Moisture in the Critical Zone of Gully Consolidation and Highland Protection. *Water* **2022**, *14*, 3674. [CrossRef]
21. Huo, A.; Wang, X.; Zhao, Z.; Yang, L.; Zhong, F.; Zheng, C.; Gao, N. Risk Assessment of Heavy Metal Pollution in Farmland Soils at the Northern Foot of the Qinling Mountains, China. *Int. J. Environ. Res. Public Health* **2022**, *19*, 14962. [CrossRef]

22. Lu, T.; Huo, A.; Wang, J.; Lu, Y.; Zhou, W. Hydrodynamic Behaviors and Geochemical Evolution of Groundwater for Irrigation in Yaoba Oasis, China. *Water* **2022**, *14*, 3924. [CrossRef]
23. Hui, S.; Wankui, N.; Haisong, L. Development Characteristics and Distribution of Earthquake-induced Loess Landslides in Xiji County of Ningxia Hui Autonomous Region. *Bull. Soil Water Conserv.* **2012**, *32*, 28–31. [CrossRef]
24. Ferretti, A.; Prati, C.; Rocca, F. Nonlinear subsidence rate estimation using permanent scatterers in differential SAR interferometry. *IEEE Trans. Geosci. Remote Sens.* **2000**, *38*, 2202–2212. [CrossRef]
25. Cheng, J.; Aidi, H.; Xinghua, Z.; Hong, W.; Xiaolu, Z.; Xiaofan, W. Research status of loess hydraulic erosion-landslide-mudflow chain. *J. Nat. Disasters* **2019**, *28*, 38–43. [CrossRef]
26. Peng, J.B.; Huo, A.D.; Cheng, Y.X.; Dang, J.; Wei, H.; Wang, X.F.; Li, C.Y. Submersion simulation in a typical debris flow watershed of Jianzhuangchuan catchment, Loess Plateau. *Environ. Earth Sci.* **2017**, *76*, 462. [CrossRef]
27. Cheng, Y.X.; Huo, A.D.; Zhao, Z.X.; Peng, J.B. Analysis of loess fracture on slope stability based on centrifugal model tests. *Bull. Eng. Geol. Environ.* **2021**, *80*, 3647–3657. [CrossRef]
28. Huo, A.D.; Peng, J.B.; Cheng, Y.X.; Zheng, X.L.; Wen, Y.R. Temporal Characteristics of the Rainfall Induced Landslides in the Chinese Loess Plateau (China). In Proceedings of the 1st Springer Conference of the Arabian-Journal-of-Geosciences (CAJG), Hammamet, Tunisia, 12–15 November 2018.
29. Huo, A.D.; Yang, L.; Peng, J.H.; Cheng, Y.X.; Jiang, C. Spatial characteristics of the rainfall induced landslides in the Chinese Loess Plateau. *Hum. Ecol. Risk Assess.* **2020**, *26*, 2462–2477. [CrossRef]
30. Crozier, M.J. A proposed cell model for multiple-occurrence regional landslide events: Implications for landslide susceptibility mapping. *Geomorphology* **2017**, *295*, 480–488. [CrossRef]
31. Zhao, H.Q.; Yi, W.; Huang, H.F.; Xia, J.B. Analysis of Water Content and Stability of Reservoir Landslides with Different Rainfall Intensities. *Saf. Environ. Eng.* **2016**, *23*, 53–58. [CrossRef]
32. Xu, G.H.; He, X.F.; Wang, G.R.; Hu, Z.Y.; Cheng, X.; Li, X.Q. InSAR identification and cause analysis of landslide disaster in Ningxia (Xiji county) section of the Yellow River basin. *Bull. Surv. Mapp.* **2022**, *68*, 104–107. [CrossRef]
33. Chen, S.M.; Huo, A.D.; Zhang, J.; Zhao, Z.Z.; Chen, S.B.; Chen, J. Identification of Potential Landslides in the Loess Hilly Area (Xiji County) of Ningxia with InSAR Technology. *Sci. Technol. Eng.* **2022**, *22*, 4721–4728.
34. Hungr, O.; Leroueil, S.; Picarelli, L. The Varnes classification of landslide types, an update. *Landslides* **2014**, *11*, 167–194. [CrossRef]
35. Yang, L.X. Causes, Characteristics and prevention strategies of landslide geological disasters in Yuanzhou District, Guyuan City, Ningxia. *China Met. Bull.* **2020**, *28*, 195–196.